

## Article

# Electrically Tunable Liquid Crystal Phase Grating with Double Period Based on the VIS Mode

Zhou Guo, Yao Li, Yu-Meng Zeng, Le Yu and Li-Lan Tian \*

School of Mathematics and Physics, Chengdu University of Technology, Chengdu 610059, China; 15639103192@163.com

\* Correspondence: tianlilan@cdut.edu.cn

**Abstract:** A tunable liquid crystal (LC) phase grating based on vertical-field in-plane electrical switching (VIS) is proposed. The tunable LC phase grating is composed of four parts: an LC layer, the top-plane and bottom-plane electrodes, the polyimide (PI) layer, and the top and bottom periodical strip electrodes. On the one hand, a large period LC phase grating can be obtained by applying voltage to the upper plane electrode and the lower periodic strip electrodes. On the other hand, a small period LC phase grating can be obtained by applying voltage to the lower plane electrode and the upper period electrodes. As a result, two kinds of LC phase grating with different periods can be realized by changing the driving scheme. Naturally, the diffraction angle can be adjusted by controlling different LC phase grating periods. The simulation results show that this tunable LC phase grating based on the VIS mode has a relatively short response time and low operating voltage (5.4 V). These characteristics make the tunable LC phase grating have good application prospects in holographic 3D or augmented reality (AR) display.

**Keywords:** liquid crystal phase grating; low voltage; vertical and in-plane switching; double period



**Citation:** Guo, Z.; Li, Y.; Zeng, Y.-M.; Yu, L.; Tian, L.-L. Electrically Tunable Liquid Crystal Phase Grating with Double Period Based on the VIS Mode. *Crystals* **2023**, *13*, 1235. <https://doi.org/10.3390/cryst13081235>

Academic Editors:  
Vladimir Chigrinov and  
Borislav Angelov

Received: 20 June 2023  
Revised: 2 August 2023  
Accepted: 8 August 2023  
Published: 10 August 2023



**Copyright:** © 2023 by the authors. Licensee MDPI, Basel, Switzerland. This article is an open access article distributed under the terms and conditions of the Creative Commons Attribution (CC BY) license (<https://creativecommons.org/licenses/by/4.0/>).

## 1. Introduction

From the perspective of visual effects, 3D display is more impressive and authentic compared with 2D display. Three-dimensional display also greatly enhances the immersion and selectivity of information [1,2]. As a dynamic 3D display, holographic 3D displays have unique advantages compared to other types of 3D displays, such as pixel-level focusing control, phase correction, and vision correction [3,4]. Therefore, holographic 3D display has become the frontier and hotspot of the present research [5]. However, due to the pixel and size limitations of spatial light modulators (SLM), the viewing angle and size of holographic images are very limited, which restricts the wide application of holographic 3D display [6,7]. To address these issues, researchers have proposed many methods, including the use of the metasurface structure [8], non-periodic photo sieve [9], and aspheric optical systems [10]. Although these methods can effectively expand the viewing angle, there are still some difficulties and challenges in their processing.

In order to solve these problems, the method of using the tunable LC phase grating has been proposed. Tunable LC phase grating has potential advantages over conventional ruled or holographic grating because of its attractive features, such as light weight, low cost, no moving parts, a large optical path difference, and the excellent light modulation ability [11–16]. It is driven by voltage to realize the adjustment of the light beam, which holds great outlook for use in holographic 3D display [17,18], optical interconnects, optical waveguides [19], and AR display [20], just to name a few. The general optical mechanism of the tunable LC phase grating is to generate the periodic electric field distribution in the LC layer. The electric field is caused by the strip pattern electrodes on the substrates of the tunable LC phase grating, after which the phase distribution of the tunable LC phase grating can be adjusted by changing the driving voltage on the electrodes. Although the tunable

LC phase gratings have these unique advantages, most of the current design structures of the tunable LC phase gratings still cannot meet the application requirements of holographic 3D displays well. For example, the viewing angle of holographic reproduction based on an SLM is generally less than  $9^\circ$  and the size is less than 2 cm [21,22], which seriously limits the widespread application of holographic 3D displays. In order to achieve a larger viewing angle and size of a holographic 3D display, many new tunable LC phase gratings have been proposed [23–25]. Nevertheless, on the one hand, due to the fact that most of the current LC grating structures are designed with periodic electrodes arranged on one side of the grating structure, it is relatively complex to achieve adjustable diffraction angles with the designed structure. On the other hand, some researchers have proposed adding periodical electrodes on both sides to achieve multi period LC grating, but their operation methods are relatively complex and difficult for wide application [26]. To improve the viewing angle and size of holographic 3D display, an adjustable LC phase grating with a simple way to control the period and the diffraction angle of the transmitted light needs to be proposed.

In this paper, we propose a tunable LC phase grating based on the VIS mode with an adjustable period under a low driving voltage (5.4 V). The tunable LC phase grating is composed of an LC layer, the top-plane and bottom-plane electrodes, the polyimide (PI) layer, and the top and bottom periodic strip electrodes. Under low operating voltage, two different types of gradient electric field are generated in the LC layer. Moreover, different modes can be selected according to corresponding driving schemes, and diffraction angle can be also controlled by modifying its driving scheme. Besides, the proposed tunable LC phase grating has a simple structure and can be produced industrially. Compared with conventional LC phase gratings, this tunable LC phase grating has a relatively fast response time and low driving voltage, making it very suitable for application in holographic 3D or AR display.

## 2. Device Structure and Principle

As shown in Figure 1a, the tunable LC phase grating comprises an LC layer, the top and bottom glass substrate, the polymer layer, the plane electrode and PI layer, and the top and bottom strip electrodes. A direct voltage  $V_{DC}$  is applied to the top and bottom plane electrodes and an alternating voltage  $V_{AC}$  is applied to the top and bottom strip electrodes. At the top of the structure, as shown in Figure 1a, the width of each electrode is  $w_{11}$ , the gap between the two bottom electrodes is  $w_{12}$ , so the grating constant of the small period LC phase grating is  $d_1 = w_{11} + w_{12}$ . At the bottom of the structure, the width of each electrode is  $w_{21}$ , the gap between two bottom electrodes is  $w_{22}$ , and thus, the grating constant of the small period LC phase grating is  $d_2 = w_{21} + w_{22}$ . All the thickness of the electrodes are the same, and the thickness of the dielectric layer both top and bottom are identical. The periodic pitch 1 and pitch 2 and the gap of the tunable LC phase grating cell are  $d_1$ ,  $d_2$ , and  $h$ , respectively.

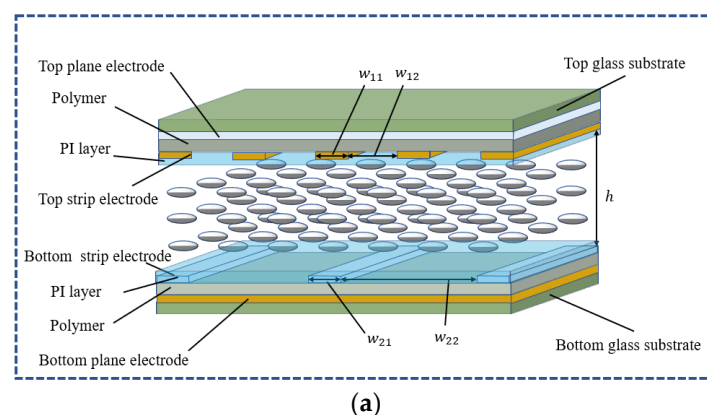
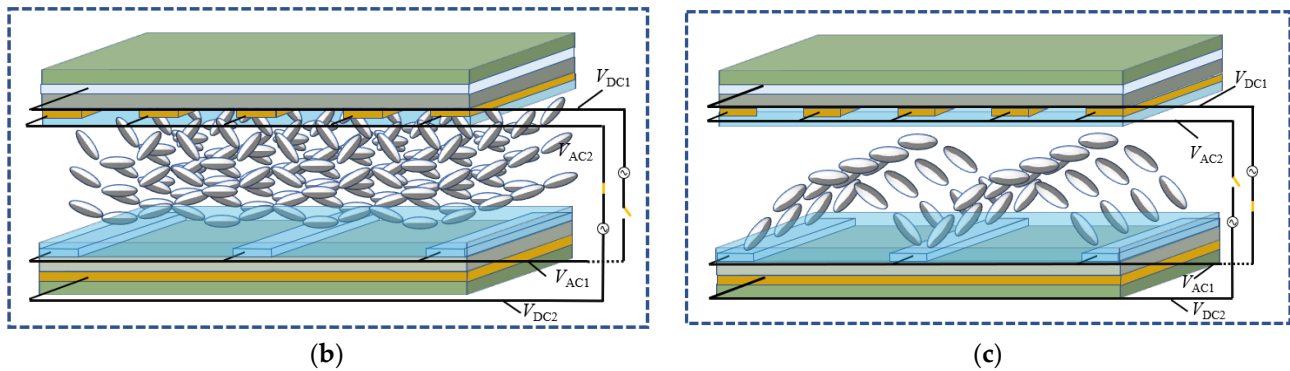


Figure 1. Cont.



**Figure 1.** The device configuration of the tunable LC phase grating with adjustable period (a). The LC director distribution within the small-period (b) and large-period (c) LC phase gratings.

All electrodes are etched with indium tin oxide (ITO) to generate a symmetrical electric field distribution under voltage-on state, which is used to generate periodic refractive index distribution. In the voltage-off state, the LC director distribution aligns homogeneously in the cell, indicating the LC layer refractive index has homogeneous distribution. When driving voltage is applied on the strip electrodes, a gradient electric field is generated in the LC layer. The LC molecules tend to align in parallel with the spatial inhomogeneous electric field direction. Therefore, different electric field distributions can be obtained through different driving schemes, and different phase distributions can be obtained. Here, two different modes of modulation can be achieved by adjusting the driving scheme. For the first driving scheme, as shown in Figure 1b, when a direct voltage  $V_{DC}$  is applied to the bottom plane electrode and an alternating voltage  $V_{AC}$  is applied to the top strip electrodes, the short-period LC phase grating can be achieved. The upper and lower electrodes form vertical electric field that change the orientation of the LC molecules at the LC layer. In this case, the bottom strip electrodes and the top plane electrode work together to generate an electric field distribution. The electric field of the LC layer from the edge to the LC grating center gradually decreases, and the LC molecules become parallel to the direction of the electric field arrangement, forming the gradient distribution center of symmetry. The phase distribution of the tunable LC phase grating is adjusted by controlling the magnitude of the  $V_{DC}$  and  $V_{AC}$ . For the second driving scheme, as shown in Figure 1c, when a direct voltage  $V_{DC}$  is applied to the top plane electrode and an alternating voltage  $V_{AC}$  is applied to the bottom strip electrodes, the large-period LC phase grating can be achieved. In this case, the top strip electrodes and the bottom plane electrode work together produce another electric field distribution, which leads to another periodic refractive index distribution. Therefore, different diffraction angles can be achieved by adjusting different driving schemes. The effective refractive index of the LC is given by the index ellipsoid equation [27,28]:

$$n_{eff}(\theta) = \frac{n_e n_o}{(n_o^2 \sin^2 \theta + n_e^2 \cos^2 \theta)^{1/2}} \quad (1)$$

where  $\theta$  stands for the angle between the incident light and the optical axis of the LC and  $n_o$  and  $n_e$  are ordinary and extraordinary light refractive indices, respectively, in the LC layer. Using the final average effective birefringence distribution, the phase difference between the center and edge of each LC phase grating can be calculated. At the voltage-on state, the LC director tends to align with the electric field, and the optical phase profile can be calculated by:

$$\Delta\varphi = \frac{2\pi}{\lambda} \int_0^h n_{eff}(x, z) dz \quad (2)$$

where  $\lambda$  represents the wavelength of the incident light, the  $x$ -axis is perpendicular to the long side direction of the strip electrode, the  $z$ -axis is parallel to the normal direction of the

substrate, and  $h$  is the thickness of the LC layer. The grating equation can be obtained as follows:

$$d\sin\theta_1 = m\lambda \quad (3)$$

where  $d$  is the grating period,  $\theta_1$  presents the diffraction angle, and  $m$  is the diffraction order.

### 3. Simulation Results and Discussion

In order to verify the performance of the proposed tunable LC phase grating and discuss its optical properties, we use commercial simulation software Tech Wiz LCD 3D (Sanayi System Co., Ltd., Incheon, Republic of Korea) and MATLAB (MathWorks Co., Ltd., Natick, MA, USA) to simulate. In the simulation, the results of all models are calculated by the Jones matrix, while the polarized light propagating along the  $z$ -axis is expressed as [29]:

$$\vec{E} = \begin{pmatrix} E_x \\ E_y \end{pmatrix} = \begin{pmatrix} E_{ox}e^{-i\varphi_x} \\ E_{oy}e^{-i\varphi_y} \end{pmatrix} \quad (4)$$

where  $E_x$  and  $E_y$  are the component of the polarized light in the  $x$ -axis and  $y$ -axis, respectively,  $E_{ox}$  and  $E_{oy}$  represent the amplitudes of polarized light in the  $x$ -axis direction and  $y$ -axis, respectively, and  $\varphi_x$  and  $\varphi_y$  are the initial phase of the polarized light, respectively. MATLAB is used to process the simulation results and draw the refractive index distribution map of the tunable LC phase grating under different conditions. Furthermore, since the grating constant (here,  $d_1 = 20 \mu\text{m}$ ,  $d_2 = 40 \mu\text{m}$ ) is much larger than the wavelength (here,  $\lambda = 550 \text{ nm}$ ), the light interference inside the grating can be neglected and the periodical boundary condition can be applied [30]. In the simulation, the numerical network is a square network with a side length of  $1 \mu\text{m}$ , and the results obtained under this setting are clear and detailed.

The LC material used in the simulation is the JC-TNLC-E7 (King Optronics Co., Ltd., Suzhou, China), with  $K_{11} = 16.7 \text{ pN}$ ,  $K_{22} = 7.3 \text{ pN}$ ,  $K_{33} = 18.1 \text{ pN}$ ,  $n_e = 1.741$ ,  $n_o = 1.517$ , the birefringence  $\Delta n = 0.224$ , dielectric constant  $\Delta\epsilon = 11.4$ , and viscosity  $\gamma = 29 \text{ mPa}\cdot\text{s}$ . The parameters of the different tunable LC phase gratings are shown in Tables 1 and 2. The grating constants  $d$  of the first type and second type tunable LC grating are  $20 \mu\text{m}$  and  $40 \mu\text{m}$ , respectively. Adjustments of the period is accomplished by changing the driving scheme. The thickness of the PI layer is  $0.1 \mu\text{m}$ , and the thickness of the electrodes and polymer layer is  $0.04 \mu\text{m}$ .

**Table 1.** Material parameters of the different tunable LC phase gratings.

Material	$\Delta n$	$\Delta\epsilon$	$\gamma$	$K_{11}$	$K_{22}$	$K_{33}$	$n_e$	$n_o$
E7-LC	0.224	11.4	29 mPa·s	16.7 pN	7.3 pN	18.1 pN	1.741	1.517

**Table 2.** Parameters of the different tunable LC phase gratings.

Type	Gap	Width	$d$	$h$	Periodic Order
1	$w_{12} = 18 \mu\text{m}$	$w_{11} = 2 \mu\text{m}$	$20 \mu\text{m}$	$10 \mu\text{m}$	Small
2	$w_{22} = 38 \mu\text{m}$	$w_{21} = 2 \mu\text{m}$	$40 \mu\text{m}$	$10 \mu\text{m}$	Large

As the voltage gradually increases, the LC molecules will gradually change their direction of deflection under the action of an electric field. When the voltage increases to a certain angle, the polarization of the LC will reach saturation, and the voltage at the time of saturation is obtained through extensive adjustment. Under this voltage condition, some characteristics of the LC phase grating are studied. On the one hand, when a direct voltage  $V_{DC} = 1 \text{ V}$  is applied to the bottom plane electrode and an alternating voltage  $V_{AC} = 5.4 \text{ V}$  is applied to the top strip electrodes, the periodical electric field distribution in small period

can be achieved because of the periodical electric field distribution. As shown in Figure 2a, the electric field distribution inside the LC layer has spatial heterogeneity and symmetry. Since electric field intensity on the edge is stronger than the LC phase grating center of electric field strength, the LC layer presents internal electric field gradient distribution. Therefore, the phase distribution can be adjusted by adjusting the internal electric field distribution. According to the simulation, the electric potential distribution is shown in Figure 2b. From the figure we can see, the electric potential lines become denser from the center to the border of the LC phase grating, so the electric field intensity becomes stronger, which indicates that the inclination angle of the LC director at the LC phase grating border is larger than that at the center. Moreover, the electric potential distribution also shows axisymmetric distribution, as shown in Figure 2b. On the other hand, when a direct voltage  $V_{DC} = 1$  V is applied to the top plane electrode and an alternating voltage  $V_{AC} = 6.2$  V is applied to the bottom strip electrodes, the large-period grating can be achieved. The electric field distribution and the electric potential distribution are shown in Figure 2c,d, respectively. From an application perspective, such a low operating voltage can meet the requirements of holographic 3D display.

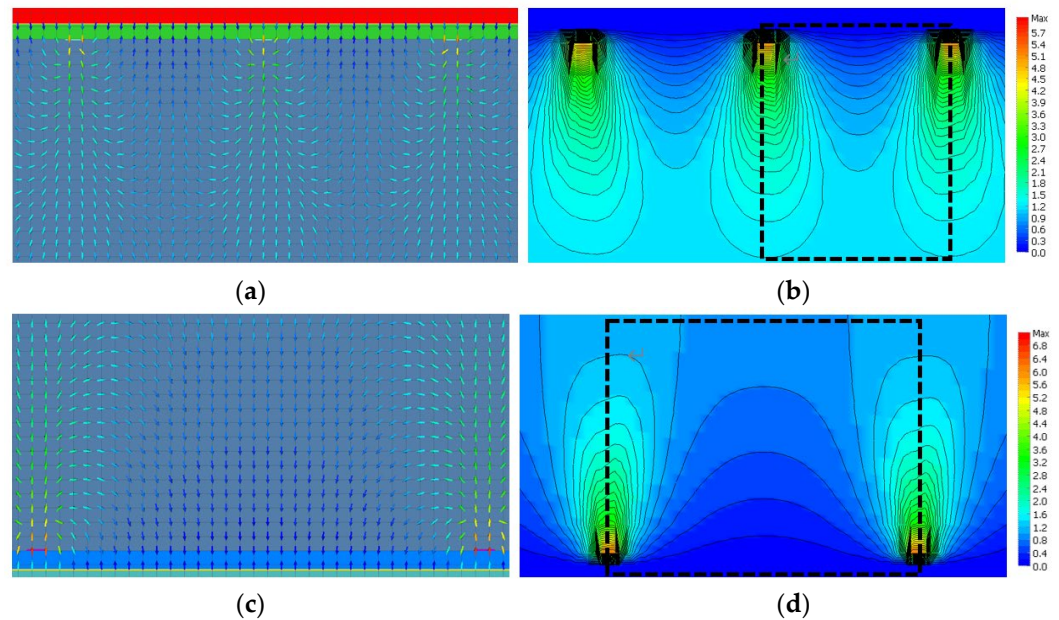


**Figure 2.** (a) Intensity distribution of the electric field distribution ( $V_{DC} = 1$  V,  $V_{AC} = 5.4$  V). (b) Distribution of the electric potential ( $V_{DC} = 1$  V,  $V_{AC} = 5.4$  V). (c) Intensity distribution of the electric field distribution ( $V_{DC} = 1$  V,  $V_{AC} = 6.2$  V). (d) Distribution of the electric potential ( $V_{DC} = 1$  V,  $V_{AC} = 6.2$  V).

In order to further study the distribution of LC molecules in the LC phase grating, the side views of the distribution of LC molecules in the small and large periods are derived, as shown in Figure 3a,b, respectively. The LC distribution area of individual LC phase grating is framed by a dotted frame, as shown in Figure 3a,b. From the figure, we can see that the angle of inclination of LC molecules at the edge is significantly greater than that of the center, indicating extraordinary light refractive index from the center  $n_e$  can gradually be reduced to the edge of  $n_o$ . Therefore, the LC layer formation with gradient refractive index distribution of LC phase grating can converge incident light. As shown in Figure 3a,b, the period of the small-period LC phase grating is half of that of the large-period LC phase grating, which indicates that the diffraction angle doubles compared to the large-period LC phase grating, since the diffraction angle is inversely proportional to the grating period when the diffraction angle is very small.

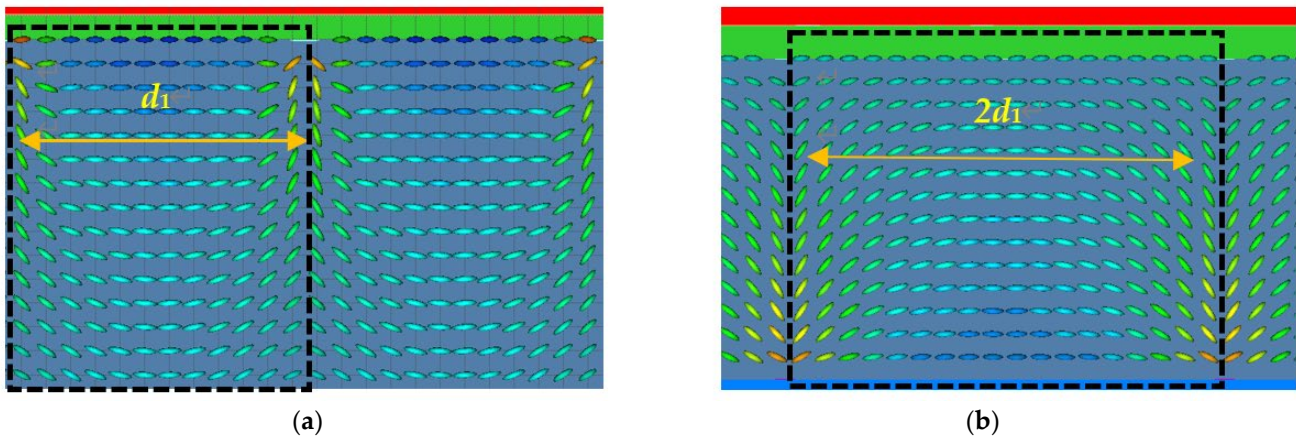


**Figure 3.** The LC director distribution (a) within a small period and (b) within a large period.

In order to better study the characteristics of the proposed tunable LC phase grating, the refractive index distribution and phase distribution of the LC phase grating are plotted under different conditions. When  $V_{DC} = 1$  V and  $V_{AC} = 5.4$  V, the profile of refraction index distribution of LC phase grating within a small period is derived. In this case, the minimum refractive index is 1.631 and the maximum refractive index is 1.732, as shown in Figure 4a. When  $V_{DC} = 1$  V and  $V_{AC} = 6.2$  V, the profile of refraction index distribution of LC phase grating within a large period is derived. In this case, the minimum refractive index is 1.575 and the maximum refractive index is 1.726, as shown in Figure 4b. Through a large number of simulation experiments, we can find that other cases have similar refractive index distribution. In order to further study the diffraction effect, we plot the phase difference distribution of in-ray polarized light in LC phase grating, compared with the ideal of the parabolic curve. For ease of understanding, we set the phase in the center of the LC phase grating to zero. LC phase grating of the phase distribution of linear polarized incident (blue solid square) and ideal parabola distribution (red solid line) are shown in Figure 4c,d. As shown in Figure 4c,d, the polarization of the incident ray of light phase distribution and the ideal parabola match very well.

As an important reference factor for grating applications, diffraction efficiency needs to be studied. Figure 5 shows the diffraction efficiency of the zeroth, first, and second orders for large-period and small-period tunable phase gratings. The diffraction efficiency is calculated as the ratio of the intensity of the diffraction order to the overall intensity without the driving voltage. The diffraction efficiency is similar for  $+m$  and  $-m$  orders. The energy transfers between the zeroth order and the higher orders by controlling the applied voltage, which provides a wide potential application for optical interconnects. For an ideal phase grating, the diffraction efficiency can be calculated as Equation (5), theoretically, where  $D$  is the active area above the strip electrodes,  $\Delta\varphi$  is the optical phase difference between the active area and the other area, and the period  $d$  equals  $d_1$  and  $d_2$  for small-period and large-period phase grating, respectively [31]:

$$\begin{cases} \eta_0 = 1 - 2\frac{D}{d}\left(1 - \frac{D}{d}\right)(1 - \cos \Delta\varphi) \\ \eta_m = \frac{1}{m^2\pi^2}\left(1 - \cos \Delta\varphi\right)\left(1 - \cos \frac{2\pi m D}{d}\right) \end{cases} \quad (5)$$

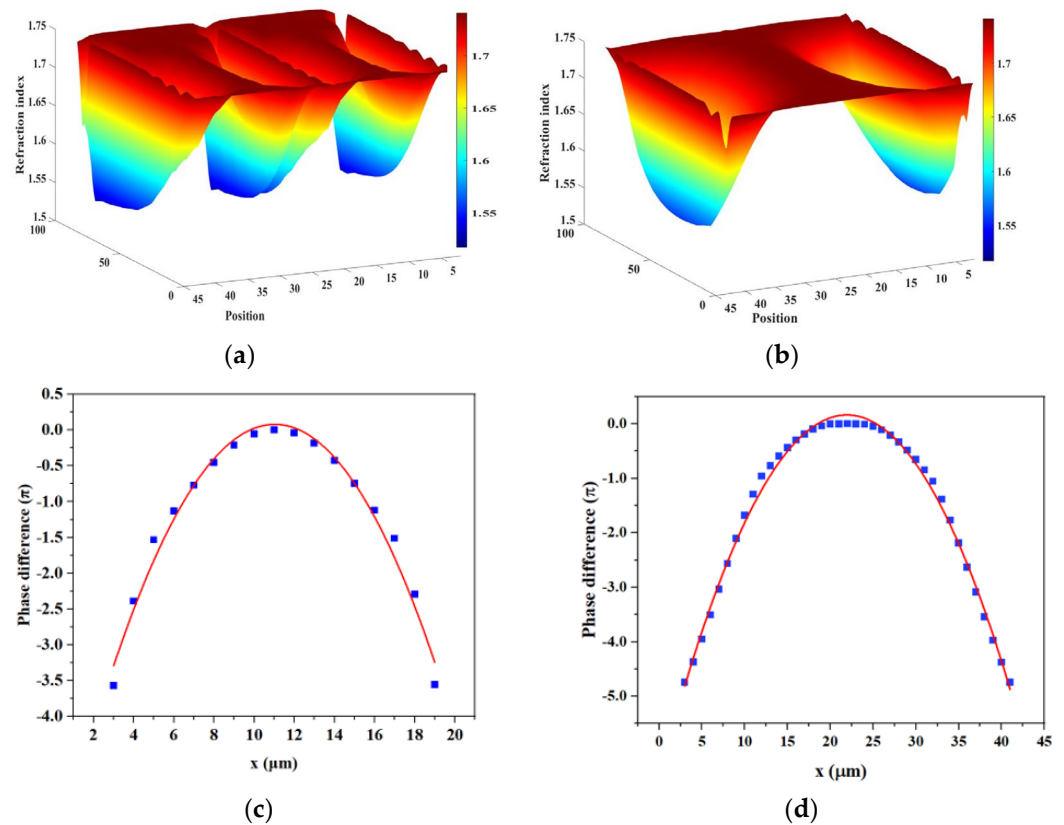


**Figure 4.** Simulated refractive index distribution profile across the tunable LC phase grating (a) within a small period, and (b) within a large period. Simulated relative phase difference profiles across the tunable LC phase grating (c) within a small period, and (d) within a large period.

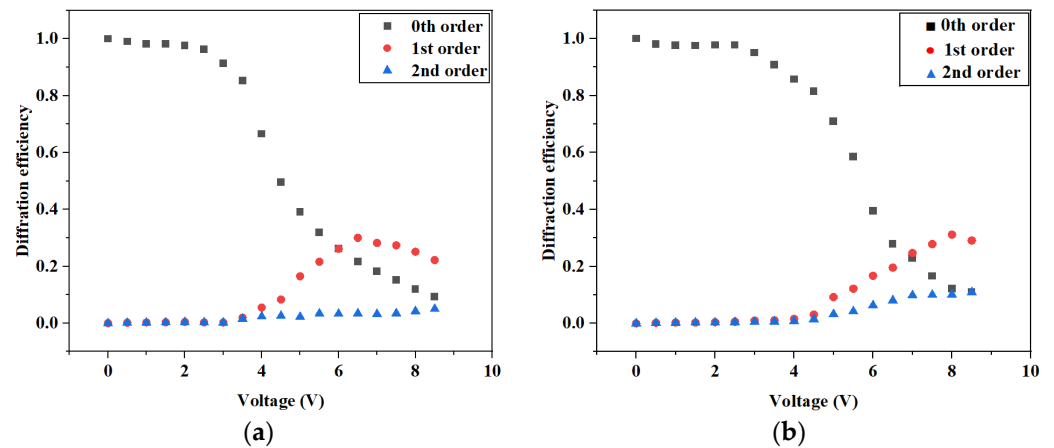


**Figure 5.** Simulation results of diffraction efficiencies of zeroth, first, and second orders. (a) Large-period phase grating and (b) small-period phase grating.

Due to the existence of the fringing electric field, the real active area is larger than the width of the strip electrodes [12]. The active area  $D$  increases with the increase of the driving voltage. Thus, during the calculation, we fit the parameter  $D$ . The value of active area  $D$  is considered to be linear change with the applied voltage. The obtained  $D$  is varied from 2 to 7  $\mu\text{m}$  for small-period phase grating, and from 2 to 28  $\mu\text{m}$  for large-period phase grating. The diffraction efficiencies under different applied voltages are under the combined effect of the change of phase difference  $\Delta\varphi$  and duty cycle. As shown in Figure 5, the first-order diffraction efficiency can reach 29.7% at 6.5 V for large-period phase grating,

and 31.1% at 8.1 V for small-period phase grating. This feature makes it more promising for optical applications.

Due to the speed of the response time is an important criterion for evaluating the quality of a device, the characteristics of the response time of tunable LC phase grating under different conditions have been studied. The response time of LC phase grating under different conditions is shown in Figure 6. The rise and decay times are defined as the times that the diffraction efficiency of the first order changed from 90% to 10% and from 10% to 90%, respectively. Firstly, by measurement, the rise time is 6.5 ms and the decay time is 15.7 ms for the applied voltage of 5 V in the case of small-period LC phase grating, as shown in Figure 6a. Moreover, the rise time is 7.8 ms and the decay time is 16.7 ms in the case of large-period LC phase grating, as shown in Figure 6b. Due to the thin thickness of the LC layer and low viscosity nematic phase LC materials, the response time is relatively fast during diffraction pattern changes, which is mainly adaptive for the holographic 3D display [32]. If tunable LC phase grating is used for faster switching, such as modulators, and filters, further improvement in dynamic response time is needed. In addition to using low viscosity LC materials, overdriven and undershoot drive schemes can also be used to accelerate response speed. Furthermore, on the one hand, the frequency convertible dielectric anisotropy of the dual frequency mixture allows us to create a fast responsive in plane switching metamaterial surface at the nanoscale, which can be tuned by electrical signals with different frequencies [33–35]. On the other hand, blue phase liquid crystal materials also have a fast response time, at a submillisecond level [36].

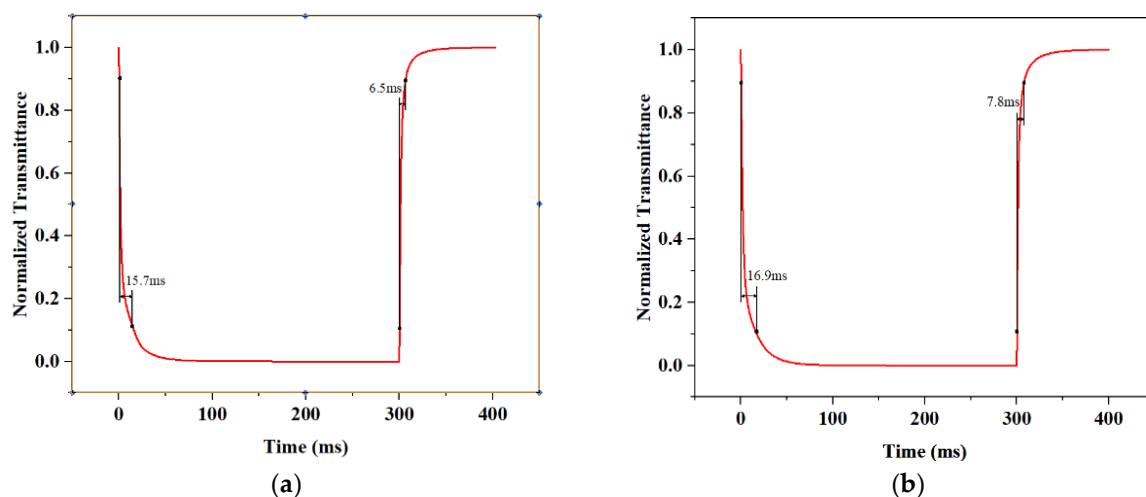


**Figure 6.** Electro-optical response of the tunable LC phase grating with different periods in rise and decay processes upon application of 5 V. (a) Small-period phase grating and (b) large-period phase grating.

#### 4. Materials and Methods

The parameters of the JC-TNLC-E7 (King Optronics Co., Ltd., Suzhou, China) material used in the simulation are as follows: elastic constant  $K_{11} = 16.7$  pN,  $K_{22} = 7.3$  pN,  $K_{33} = 18.1$  pN, refractive indices of  $o$  and  $e$  waves  $n_e = 1.741$  and  $n_o = 1.517$ , respectively, dielectric anisotropy  $\Delta\epsilon = 11.4$ , birefringence  $\Delta n = 0.224$ , and viscosity  $\gamma = 29$  mPa·s.

To validate the performance of the proposed tunable LC phase grating, we carried out electro-optical simulation using commercial simulation software Tech Wiz LCD 3D (Sanayi System Co., Ltd., Incheon, Republic of Korea) and MATLAB (MathWorks Co., Ltd., Natick, MA, USA) and performed the numerical calculations.

## 5. Conclusions

We demonstrate tunable LC phase grating with an adjustable period based on VIS modes. The LC phase grating period and the diffraction angle can be alternatively tuned through controlling the driving scheme. For each period of LC phase grating, the diffraction efficiency and phase distribution can be adjusted by changing the applied voltage and intensity of applied voltage. Relatively high efficiencies of 31.1% for the small-period phase grating and 29.7% for the large-period phase grating have been achieved. Compared to tunable LC gratings made of blue phase liquid crystal materials, the driving voltage required for the proposed grating is very low (5.4 V). Besides, the tunable LC phase grating possesses the characteristic of a relatively fast response time, entirely meeting the needs of synchronous control. Compared to traditional systems with a single SLM, the holographic display achieved by combining the proposed tunable LC phase grating can increase the viewing angle obviously. In a nutshell, the tunable LC phase grating shows great application prospects in holographic 3D and AR displays.

**Author Contributions:** Z.G. and L.-L.T. conceived the original idea and wrote the paper; Y.L. and Y.-M.Z. analyzed the data; L.Y. performed the analysis. All authors have read and agreed to the published version of the manuscript.

**Funding:** This research was funded by Sichuan Natural Science Foundation (NSFSC) (Grant No 2023NSFSC1306).

**Data Availability Statement:** Data underlying the results presented in this paper are not publicly available at this time but may be obtained from the authors upon reasonable request.

**Conflicts of Interest:** The authors declare no conflict of interest.

## References

1. Ren, H.; Shao, W.; Li, Y.; Salim, F.; Gu, M. Three-dimensional vectorial holography based on machine learning inverse design. *Sci. Adv.* **2020**, *6*, eaaz4261. [[CrossRef](#)] [[PubMed](#)]
2. Lu, J.-G.; Sun, X.-F.; Song, Y.; Shieh, H.-P.D. 2-D/3-D Switchable Display by Fresnel-Type LC Lens. *J. Disp. Technol.* **2011**, *7*, 215–219. [[CrossRef](#)]
3. Wakunami, K.; Hsieh, P.-Y.; Oi, R.; Senoh, T.; Sasaki, H.; Ichihashi, Y.; Okui, M.; Huang, Y.-P.; Yamamoto, K. Projection-type see-through holographic three-dimensional display. *Nat. Commun.* **2016**, *7*, 12954. [[CrossRef](#)] [[PubMed](#)]
4. Wang, D.; Li, N.-N.; Li, Y.-L.; Zheng, Y.-W.; Nie, Z.-Q.; Li, Z.-S.; Chu, F.; Wang, Q.-H. Large viewing angle holographic 3D display system based on maximum diffraction modulation. *Light Adv. Manuf.* **2023**, *4*, 18. [[CrossRef](#)]
5. Shi, L.; Li, B.; Kim, C.; Kellnhofer, P.; Matusik, W. Towards real-time photorealistic 3D holography with deep neural networks. *Nature* **2021**, *591*, 234–239. [[CrossRef](#)]
6. Ghaith, M.; Özgün, Y.; Kesim, D.K.; Ahmet, T.; Parviz, E.; Serim, L.; Llday, T.O. Breaking crosstalk limits to dynamic holography using orthogonality of high-dimensional random vectors. *Nat. Photonics* **2019**, *13*, 251–256.
7. Peng, Y.; Choi, S.; Kim, J.; Wetzstein, G. Speckle-free holography with partially coherent light sources and camera-in-the-loop calibration. *Sci. Adv.* **2021**, *7*, eabg5040. [[CrossRef](#)]
8. Gao, H.; Wang, Y.; Fan, X.; Jiao, B.; Li, T.; Shang, C.; Zeng, C.; Deng, L.; Xiong, W.; Xia, J.; et al. Dynamic 3D meta-holography in visible range with large frame number and high frame rate. *Sci. Adv.* **2020**, *6*, eaba8595. [[CrossRef](#)]
9. Park, J.; Lee, K.; Park, Y. Ultrathin wide-angle large-area digital 3D holographic display using a non-periodic photon sieve. *Nat. Commun.* **2019**, *10*, 1304. [[CrossRef](#)]
10. Li, Q.; Li, Y.; Ma, J.; Yang, D.-K.; White, T.J.; Bunning, T.J. Directing Dynamic Control of Red, Green, and Blue Reflection Enabled by a Light-Driven Self-Organized Helical Superstructure. *Adv. Mater.* **2011**, *23*, 5069–5073. [[CrossRef](#)] [[PubMed](#)]
11. Gilardi, G.; De Sio, L.; Beccherelli, R.; Asquini, R.; D'alessandro, A.; Umerton, C. Observation of tunable optical filtering in photosensitive composite structures containing liquid crystals. *Opt. Lett.* **2011**, *36*, 4755–4757. [[CrossRef](#)]
12. Xu, D.; Tan, G.; Wu, S.-T. Large-angle and high-efficiency tunable phase grating using fringe field switching liquid crystal. *Opt. Express* **2015**, *23*, 12274–12285. [[CrossRef](#)] [[PubMed](#)]
13. Chen, J.; Bos, P.J.; Vithana, H.; Johnson, D.L. An electro & hyphen optically controlled liquid crystal diffraction grating. *Appl. Phys. Lett.* **1995**, *67*, 2588–2592.
14. Friedman, L.J.; Hobbs, D.S.; Lieberman, S.; Corkum, D.L.; Nguyen, H.Q.; Resler, D.P.; Sharp, R.C.; Dorschner, T.A. Copy-right 2006 society of photo instrumentation engineers. *Proc. IEEE* **1996**, *84*, 268–298.
15. Dou, H.; Wang, L.; Xu, L.-P.; Mao, X.; Ou, J.-Y.; Nie, J.-Y.; Wang, S.-R.; Wang, S.; Dan, Y.-Q. Directional modulated light-emitting technology based on airborne display. *Liq. Cryst.* **2022**, *49*, 2146–2154. [[CrossRef](#)]

16. Ren, H.; Fan, Y.-H.; Wu, S.-T. Prism grating using polymer stabilized nematic liquid crystal. *Appl. Phys. Lett.* **2003**, *82*, 3168–3170. [[CrossRef](#)]
17. Algorri, J.F.; Urruchi, V.; Bennis, N.; Sánchez-Pena, J.M. Cylindrical liquid crystal micro-lens array with rotary axis and tunable capability. *IEEE Electron Device Lett.* **2015**, *36*, 582–584. [[CrossRef](#)]
18. Chu, F.; Guo, Y.-Q.; Zhang, Y.-X.; Duan, W.; Zhang, H.-L.; Tian, L.-L.; Li, L.; Wang, Q.-H. Four-mode 2D/3D switchable display with a 1D/2D convertible liquid crystal lens array. *Opt. Express* **2021**, *29*, 37464–37475. [[CrossRef](#)]
19. Gilardi, G.; Asquini, R.; D’Alessandro, A.; Beccherelli, R.; De Sio, L.; Umeton, C. All-Optical and Thermal Tuning of a Bragg Grating Based on Photosensitive Composite Structures Containing Liquid Crystals. *Mol. Cryst. Liq. Cryst.* **2012**, *558*, 64–71. [[CrossRef](#)]
20. Chang, C.; Bang, K.; Wetzstein, G.; Lee, B.; Gao, L. Toward the next-generation VR/AR optics: A review of holographic near-eye displays from a human-centric perspective. *Optica* **2020**, *7*, 1563–1578. [[CrossRef](#)]
21. Blanche, P.-A. Holography, and the future of 3D display. *Light Adv. Manuf.* **2021**, *2*, 28. [[CrossRef](#)]
22. Yu, H.; Lee, K.; Park, J.; Park, Y. Ultrahigh-definition dynamic 3D holographic display by active control of volume speckle fields. *Nat. Photonics* **2017**, *11*, 186–192. [[CrossRef](#)]
23. Simeon, S.; Margarita, M.; Marga, P.; Dimitar, T. Holographic diffraction grating controlled by means of nematic liquid crystal. *Mol. Cryst.* **1987**, *152*, 609–615.
24. Dou, H.; Wang, L.; Ren, G.; Dan, Y.-Q.; Zhong, X.-T.; Ou, J.-Y.; Yuan, J.-Y.; Zhong, Y.-T. A Light-Mixing Liquid Crystal Lens-Like Cell to Decrease Color Shift and Tune Brightness for Displays. *Crystals* **2022**, *12*, 213. [[CrossRef](#)]
25. Caputo, R.; De Sio, L.; Veltri, A.; Umeton, C.; Sukhov, A.V. Development of a new kind of switchable holographic grating made of liquid-crystal films separated by slices of polymeric material. *Opt. Lett.* **2004**, *29*, 1261–1263. [[CrossRef](#)]
26. Gu, L.; Chen, X.; Jiang, W.; Howley, B.; Chen, R.T. Fringing-field minimization in liquid-crystal-based high-resolution switchable gratings. *Appl. Phys. Lett.* **2005**, *87*, 201106. [[CrossRef](#)]
27. Wang, B.; Ye, M.; Sato, S. Liquid Crystal Negative Lens. *Jpn. J. Appl. Phys.* **2005**, *44*, 4979–4983. [[CrossRef](#)]
28. Dou, H.; Chen, M.; Li, D.; Yu, G.; Sun, Y.-B. A controllable viewing angle optical film using micro prisms filled with liquid crystal. *Liq. Cryst.* **2021**, *48*, 1373–1381. [[CrossRef](#)]
29. Lien, A. The general and simplified Jones matrix representations for the high pretilt twisted nematic cell. *J. Appl. Phys.* **1990**, *67*, 2853–2856. [[CrossRef](#)]
30. Li, J.-N.; Hu, X.-K.; Wei, B.-Y.; Wu, Z.-J.; Ge, S.-J.; Ji, W.; Hu, W.; Lu, Y.-Q. Simulation and optimization of liquid crystal gratings with alternate twisted nematic and planar aligned regions. *Appl. Opt.* **2014**, *53*, E14–E18. [[CrossRef](#)]
31. Magnusson, R.; Gaylord, T.K. Diffraction efficiencies of thin phase gratings with arbitrary grating space. *J. Opt. Soc. Am. A.* **1978**, *68*, 806–809. [[CrossRef](#)]
32. Xiong, J.; Hsiang, E.-L.; He, Z.; Zhan, T.; Wu, S.-T. Augmented reality and virtual reality displays: Emerging technologies and future perspectives. *Light Sci. Appl.* **2021**, *10*, 216. [[CrossRef](#)] [[PubMed](#)]
33. Kowrdziej, R.; Wróbel, J.; Kula, P. Ultrafast electrical switching of nanostructured metadvice with dual-frequency liquid crystal. *Sci. Rep.* **2019**, *9*, 20367. [[CrossRef](#)] [[PubMed](#)]
34. Golovin, A.B.; Shiyanovskii, S.V.; Lavrentovich, O.D. Fast switching dual-frequency liquid crystal optical retarder, driven by an amplitude and frequency modulated voltage. *Appl. Phys. Lett.* **2003**, *83*, 3864–3866. [[CrossRef](#)]
35. Xianyu, H.; Wu, S.-T.; Lin, C.-L. Dual frequency liquid crystals: A review. *Liq. Cryst.* **2009**, *36*, 717–726. [[CrossRef](#)]
36. Yan, J.; Li, Y.; Wu, S.-T. High-efficiency and fast-response tunable phase grating using a blue phase liquid crystal. *Opt. Lett.* **2011**, *36*, 1404–1406. [[CrossRef](#)]

**Disclaimer/Publisher’s Note:** The statements, opinions and data contained in all publications are solely those of the individual author(s) and contributor(s) and not of MDPI and/or the editor(s). MDPI and/or the editor(s) disclaim responsibility for any injury to people or property resulting from any ideas, methods, instructions or products referred to in the content.